THE JOURNAL OF PHYSICAL CHEMISTRY C

Article

pubs.acs.org/JPCC

Relaxation Dynamics and Structural Characterization of Organic Nanobelts with Aggregation-Induced Emission

Chih-Wei Chang,*[,†] Chetan Jagdish Bhongale,[‡] Chi-Shen Lee,[‡] Wei-Kai Huang,[‡] Chain-Shu Hsu,[‡] and Eric Wei-Guang Diau*[,‡]

[†]Department of Chemistry, National Changhua University of Education, Changhua 50058, Taiwan

[‡]Department of Applied Chemistry and Institute of Molecular Science, National Chiao Tung University, Hsinchu 30010, Taiwan

Supporting Information

ABSTRACT: We prepared the fluorescent nanobelts of cyano-substituted 1,4-distyrylbenzene derivative (CNDSB) with the reprecipitation method. CNDSB is nonemissive in solution but with strong aggregation-induced emission (AIE) in belt-like structure. The molecular structure predicted by quantum chemical calculations indicates a twisted conformation of CNDSB monomer, while the solid-state X-ray structure of the CNDSB crystal features herringbone-type arrangement and three benzene rings arrange in nearly planar conformation. Femto- and picosecond time-resolved fluorescence spectroscopy are implemented to study the photophysics and the origin of the AIE effect in CNDSB nanobelts. The fluorescence quenching of CNDSB in THF solution arises from the efficient nonradiative isomerization channel. In this study, the fluorescence decay of CNDSB embedded in poly(methyl methacrylate) matrix is slowed down due to the restriction of intramolecular motions in the solid matrix. In nanobelt structure, the fluorescence lifetime further increases due to the intermolecular interaction between H-type aggregates. Both the steady-state and time-resolved studies suggests that there are at least two different packing structures might exist in nanobelts, and the relative composition of these two different structures gradually changes in different sizes of nanobelts.

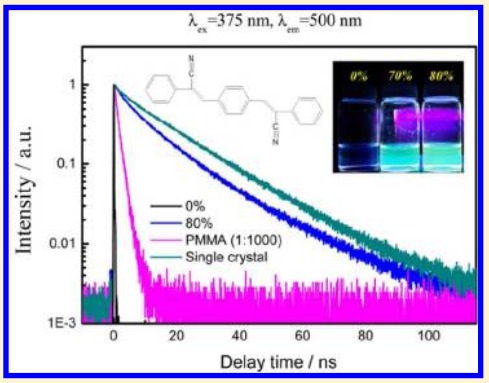

INTRODUCTION

Over the past decades, different kinds of luminescent nanoparticles have been prepared and extensively studied because of their applications to organic light-emitting devices,[1−3] nanosensors,[3,4] and the detection of DNA conformation changes.[5,6] Nanoparticles have attracted lots of attention due to their special properties between individual molecules and those of bulk materials.[7] The weak intermolecular forces and the hydrogen bond between organic molecules[8] make the electronic properties of organic nanoparticles fundamentally different from that of inorganic materials.[9−11] Organic compound provides the variability and flexibility in the synthesis of new materials, preparing of nanostructures, and investigating of their photophysical properties.[12−15] Organic nanocrystals are expected to be used as novel functional materials in the field of electronics and photonics.[4,16,17] Nanoparticles are fascinating because of their size-dependent optical properties.[18−25] The size-dependent changes in absorption and emission spectra of organic nanoparticles arise from multiple factors such as aggregate effect,[25−27] surface effect,[27] and the increasing of intermolecular interaction induced by the change of lattice.[19,28] Many conventional organic molecules are highly emissive in dilute solution; however, the emission is drastically quenched in solid state due to the formation of exciton or excimer species.[2,29,30] The aggregation-induced quenching is deleterious for their application as luminescent materials; hence, it is desirable to develop the luminophore that can overcome this problem. The materials with the aggregation-induced emission (AIE) feature seem to be promising to solve this problem. Therefore, it has attracted lots of attention in recent years.[2,3]

Enhanced emission due to aggregation have been reported in many organic systems such as PPB,[26] *p*-BSP,[31] silole derivatives,[32−35] conjugated polymers,[36] and π-conjugated CN derivatives.[37−44] For the molecules with AIE phenomenon, the fluorescence is weak in solution and the intensity increases several order of magnitudes in solid state. Among these studies, π-conjugated cyano-substituted compounds have attacted special attention becasuse it forms fascinating 1D and 2D nanowire structures and can be used to fabricate various types of nanoelectronic devices.[42] Recent studies suggested that certain cyano-substituted organic compound also shows a unique piezochromic phenomenon.[41,43] The origin of AIE effect has been extensively investigated, and early studies suggested that the restriction of intramolecular twisting motions is the primiary reason that should response for the observing AIE phenomenon.[2,3,45,46] Meanwhile, the planarization and intermolecular force interaction is also important for

Received: April 29, 2012
Revised: June 18, 2012
Published: June 21, 2012

ACS Publications © 2012 American Chemical Society

the AIE phenomenon of cyano-substituted compounds.[39,40,42] Among these studies, the understanding of the optical properities of organic nanostructure rely on the measurements of steady-state absorption and emission spectra. Although there are several reports about the time-resolved fluorescence studies,[26,33,47] the understanding about their excited-state dynamics, especially when those molecules aggregate into nanostructures, is still limited.

On the basis of femtosecond (fs) and picosecond (ps) time-solved spectral methods, we have reported the relaxation dynamics of nanoparticles of 1,4-di[(*E*)-2-phenyl-1-propenyl]-benzene (PPB).[26] In the present work, we will report the complete spectral and dynamical characterizations of the molecule (*Z*)-3-{4-[(*Z*)-2-cyano-2-phenyl-1-ethenyl]phenyl}-2-phenyl-2-propenenitrile (CNDSB, Scheme 1), which belongs

Scheme 1

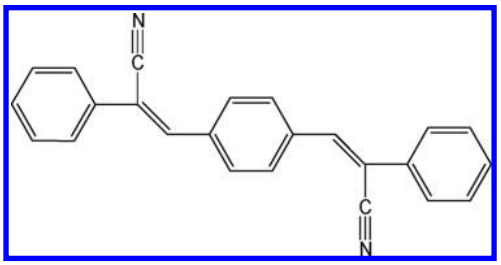

to the family of oligophenylenevinylenes with two cyano groups attached to 1,4-distyrylbenzene skeleton. CNDSB exhibits very high fluorescence quantum yield in solid state, and the CNDSB-based single crystal organic light-emitting device shows promising electroluminescence properties.[44] In contrast to PPB nanoparticles, CNDSB forms one-dimensional belt-like structure in water/THF cosolvents as the volume fraction of water in water/THF solution exceeds 70%. Like many cyano-substituted compounds, CNDSB is nonemissive in THF solution alone, but the fluorescence intensity increases several orders of magnitude when forming nanobelts. In this study, a series of time-resolved experiments were performed to elucidate the excited-state dynamics of isolated and aggregated molecules. The excited-state dynamics and the origin of the AIE phenomenon will be addressed in detail. In nanobelt structure, the steady-state and time-resolved studies suggest at least two different packing structures coexist in nanobelts. The implement of femtosecond time-resolved spectroscopy also enables us observed a unique ultrafast decay component in CNDSB nanobelts, whereas this ultrafast component was absent in PPB nanoparticles.[26]

EXPERIMENTAL SECTION

Materials. CNDSB was synthesized by Knoevenagel reaction.[48] Typically, KOH (4.2 g, 75.14 mmol) was added to a solution of terephthaladehyde (5.0 g, 37.20 mmol) and phenylacetonitrile (8.8 g, 75.14 mmol) in ethanol (50 mL). A greenish-yellow gel-type mixture was formed immediately after addition. The resulting solution was stirred for overnight at room temperature. The mixture was then filtered and washed several times by ethanol. The crude was recrystallized from chloroform to give greenish-yellow solid (yield, 45%). ^{1}H NMR (300 MHz, $CDCl_3$): δ = 8.00 (s, 2H; Ar−H), 7.72−7.7.69 (m, 4H; Ar−H), 7.56 (s, 2H; Ar−H), 7.47−7.44 (m, 6H; Ar−H), 7.26 (s, 2H; vinyl); mp 270−272 °C. EI-MS (Micromass, Trio2000) for $CNDSB^+$ (m/z): 332.

Formation of Nanostructures. CNDSB nanostructures were obtained by a simple reprecipitation method. Water served as a precipitating solvent for CNDSB in THF (99.5%, spectroscopy grade, Merck). Distilled water and THF were filtered with a membrane filter (pore size 0.2 μm). Volume fractions of water were added up to 90%, with vigorous stirring at 296 K. The concentration of chromophore (3.6×10^{-5} M) was constant after the addition of distilled water. To see the concentration dependence on the nanostructures formation of CNDSB, another series with different concentrations, 1.8×10^{-5}, 3.6×10^{-5}, and 7.2×10^{-5} M, were prepared. These suspensions were homogeneous and stable. Samples for SEM tests were prepared by dropping the sample mixture onto a microscopic glass or carbon tape and dried under vacuum.

Preparation of PMMA Thin Film. CNDSB was dissolved in $CHCl_3$ and mixed with poly(methyl methacrylate) (PMMA) at the weight ratio of CNDSB/PMMA = 1:1000. The mixture of 1:1000 CNDSB/PMMA solutions was spin-coated on quartz then evaporated the solvent.

Scanning Electron Microscopy and Steady-State Spectroscopy Measurements. Images were acquired on a field-emission scanning electron microscope (JSM-6500 F, JEOL); to enhance the conductivity of the specimen, a layer of platinum was sputtered for 30 s at a current 30 mA and a pressure 4 Pa. UV−vis absorption spectra of CNDSB in THF and PMMA film were measured with Cary 50 (Varian) spectrometer. The sample of CNDSB in THF solution was placed in a standard 1 cm cuvette while the PMMA film was placed on a solid sample holder. To avoid the scattering from nanoaggregates, the absorption spectra of CNDSB in 70%, 80%, and 90% water/THF solutions were taken with Shimadzu UV-3600 spectrometer equipped with integration sphere. The fluorescence spectra (Hitachi F4500 spectrophotometer) of solution samples were measured with standard 1 cm cuvette, and PMMA film was placed on a solid-state sample holder (model: 650-0161); the excitation wavelength was fixed at 375 nm, and all intensity has been normalized according to the absorbance at 375 nm.

Single-Crystal XRD Collection. Single crystal suitable for the X-ray diffraction study was observed from the vapor phase by sublimation. About 100 mg of CNDSB was used for the single-crystal growth, which was placed in a silica tube (i.d./o.d. = 0.9/1.1 cm; l = 30 cm) and sealed under vacuum ($P < 10^{-4}$ Torr). The silica tube was heated at 200 °C followed by slow cooling at 15/h to 100 °C in a tube furnace. The crystal showed plate-shaped morphologies and light green color and was mounted on the tips of glass fibers. Crystal quality was checked by rotation photographs on a Nonius CAD4 single crystal diffractometer with Mo Kα radiation (λ = 0.710 73 Å) at room temperature (298(2) K). Diffraction data for detailed structural analyses were collected at 100(2) K using a Bruker APEX CCD diffractometer with monochromatic Mo Kα radiation, λ = 0.710 73 Å, and a detector-to-crystal distance of 5.00 cm. The diffraction data were collected in a hemisphere and harvested by collecting four sets of frames with 0.3° scans in w for an exposure time of 60 s per frame. The range of 2θ values was 3.0°−56.3°. The data were corrected for Lorentz and polarization effects. The unit cell parameters were determined from 90 frames of reciprocal space images and then least-squares refined with all observed intensity data. The data acquisition and cell reduction were performed using SMART,

dx.doi.org/10.1021/jp304117n | J. Phys. Chem. C 2012, 116, 15146−15154

and further data reduction and integration were done with SAINTPLUS software packages. Absorption corrections were based on fitting a function to the empirical transmission surface as sampled by multiple equivalent measurements. The crystal revealed a orthorhombic unit cell (a = 19.500(12) Å, b = 6.929(4) Å, c = 26.031(16) Å, V = 3517(4) Å^3), and the systematic absences suggested space group of $Pna2_1$ (No. 33). The structure model was obtained by direct methods and refined by full-matrix least-squares refinement based on F^2 using the SHELXTL5.12 package. The structure refinement parameters for CNDSB crystal are tabulated in Table 1. The .cif file is available in the Supporting Information.

Table 1. Structure Refinement Parameters for CNDSB Crystal[a]

empirical formula	$(C_{24}H_{16}N_2)_2$
formula weight	664.78
crystal system	orthorhombic
space group	$Pna2_1$
T/K	273(2)
a/Å	19.50(1)
b/Å	6.929(4)
c/Å	26.03(2)
V/Å^3	3517(4)
Z	4
D_{calcd}/g cm^{-3}	1.255
absorption coefficient/mm^{-1}	0.074
R_{int}	0.0985
data/restraints/parameters	6206/1/439
R_1, wR_2 [$I > 2\sigma(I)$]	0.0948, 0.2384
R_1, wR_2 (all data)	0.1099, 0.2529
goodness-of-fit on F^2	1.048
largest diff peak and hole (e/ Å^3)	1.040, −0.591

[a] $R_1 = ||F_o| - |F_c||/|F_o|$; $wR_2 = [w(F_o^2 - F_c^2)^2/w(F_o^2)^2]^{1/2}$.

Femtosecond Temporally Resolved Measurements. Femtosecond temporally resolved spectra were obtained with an fluorescence optically gated system (FOG100, CDP) for fluorescence in combination with a mode-locked Ti:sapphire laser (Coherent, Mira 900D). The detailed experiment setup were described elsewhere.[26] The femtosecond laser system generates output pulses of duration ~150 fs (the full width at half-maximum of autocorrelation, fwhm) at a repetition rate 76 MHz. The spectral bandwidth of the laser is 10−12 nm, and the peak wavelength is fixed at 750 nm. The frequency of the laser pulse is doubled with a Beta-Barium (BBO) crystal (type I) and used for excitation. The instrument response function (IRF) of the up-conversion system is ~220 fs (fwhm).

Picosecond Temporally Resolved Measurements. Picosecond temporally resolved spectra were obtained with a time-correlated single-photon counting (TCSPC) system (Fluotime 200, PicoQuant). The excitation source was provided by a 375 nm picosecond pulsed-diode laser (LDH-375, PicoQuant), which controlled by a picosecond pulsed laser driver (PDL800-D, PicoQuant). The excitation laser was focused onto the sample holder by lens. A lens collected fluorescence emitted from the sample at a right angle. An iris was used to attenuate the intensity of the detected signal, and the polarization of the detected fluorescence relative to the excitation laser pulse was set at 54.7° (magic angle) with a polarizer. A double monochromator compensated the GVD of fluorescence and selected the detection wavelength. A multi-channel-plate photomultiplier was connected to a computer with a TCSPC-module (SPC-630, Becker and Hickl) card for data acquisition.

Computational Methods. The structures of isolated CNDSB molecule was optimized with density-functional theory (DFT) methods implemented in the G03 software package.[49] The ground state geometry was optimized at the B3LYP/6-31G(d) level of theory with vibrational frequencies calculated at the same level being all positive numbers. The vertical excitation energy of optimized structure is calculated with time-dependent density function theory (TDDFT) method at the B3LYP/6-31G(d) level of theory. For the cis/trans isomers in crystal, the X-ray structure is used to calculate excitation energy of these two isomers, and results are summarized in Table 2.

Table 2. Vertical Excitation Energy of Free CNDSB and Two Structural Isomers Found in Crystal Structure[a]

		free CNDSB	X-ray trans form	X-ray cis form
S_1	E	3.0098 (411.94 nm)	3.0732 (403.43 nm)	3.1024(399.63 nm)
	f	1.5110	1.4440	1.5194
S_2	E	3.5114 (353.09 nm)	3.5530 (348.96 nm)	3.5611 (348.16 nm)
	f	0.0000	0.0001	0.0013
S_3	E	3.6427 (340.36 nm)	3.6987 (335.21 nm)	3.6582 (338.92 nm)
	f	0.0063	0.0056	0.0048

[a] The excitation energy (E in eV) and the oscillator strength (f) were calculated using the TDDFT method at the B3LYP/6-31g(d) level.

RESULTS AND DISCUSSION

Formation of CNDSB Nanostructures. CNDSB nanostructures were prepared in a series of water/THF solutions (concentration = 3.6 × 10^{-5} M) with different volume fractions of water. When water is added into THF solution, it is transparent in the beginning then become milky as the volume fraction of water exceeds 70%. Figure 1 shows the scanning electron microscopy (SEM) images of CNDSB in different percentage of water/THF solutions. With the increasing of water ratio, the structure gradually evolves from zero-dimensional nanoparticle to one-dimensional belt-like structure (Figure 1a−c). The concentration effect has been tested in 80% solution. The result (Figure 1d: 1.8 × 10^{-5} M; Figure 1b: 3.6 × 10^{-5} M, Figure 1e: 7.2 × 10^{-5} M) indicates that the increasing of CNDSB concentration will increase the width of nanobelts from ~150 to ~300 nm. As a comparison, the SEM image of the powder scratched from bulk crystal is shown in Figure 1f.

Steady-State Absorption/Emission Spectra. Figures 2a and 2b are the UV−vis absorption and emission spectra of CNDSB in various conditions. The absorption of CNDSB in pure THF solution featured with a strong absorption band central at 364 nm. In 70−90% solutions, the tail at the visible region of the spectra suggests the formation of nanostructure in these solutions. In 70% solution, the peak of the absorption spectrum is shifted to about 350 nm, and the absorbance decreases substantially. In 80% solution, with the formation of nanobelt structure, a new band forms at ~320 nm, and this band further evolves to a sharp peak central at ~314 nm in 90% solution. The distinctive hypsochromic shift of the absorption spectra in 70%−90% solutions indicates the formation of H-type aggregates.[29,50] In 2010, Park et al. reported that the absorption spectrum of H-type aggregates would be drastically

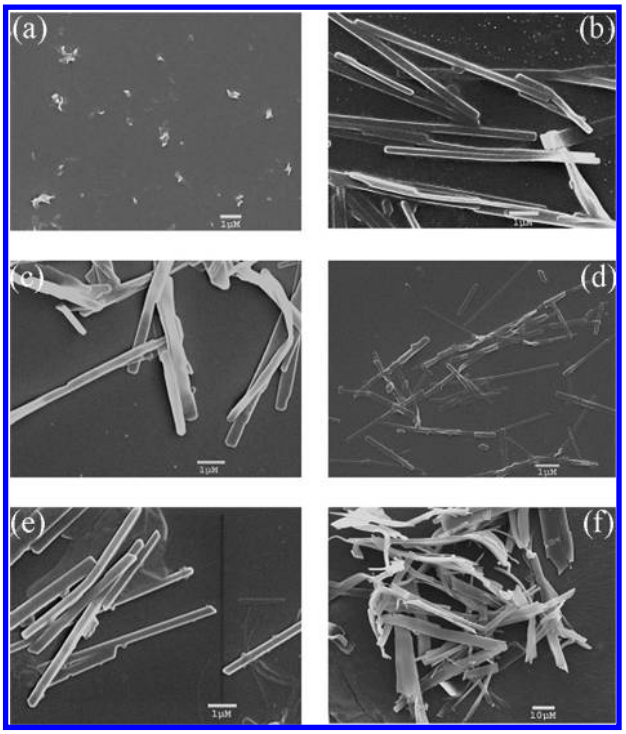

Figure 1. SEM images showing the evolution of CNDSB nanostructures obtained at different water/THF volume fractions. Concentrations of 3.6×10^{-5} M CNDSB in (a) 70, (b) 80, and (c) 90% of water/THF solution; (d) 1.8×10^{-5} M and (e) 7.2×10^{-5} M of CNDSB in 80% solution; (f) CNDSB crystal powders.

changed in different packing structures.[40] In their studies, the packing structures of H-type aggregate can be classified into two different phases: G-phase and B phase. In contrast to B-phase structure, the molecular sheets in G-phase structure are arranged in slip stack along the long molecular axis with smaller pitch angle.[40] The sliding of the molecular sheet will reduce the exciton coupling of the H-type aggregates. Thus, the hypsochromic shift of the absorption spectrum in G-phase structure will significantly less than that in B-phase structure.[40] Our result suggest the pack structure might gradually evolve from the G-phase packing (70% solution) to B-phase packing in nanobelts.

The emission of CNDSB in pure THF solution shows weak emission and clear structures around 425 and 445 nm (Figure 2b). In 70% solution, the structure of emission spectra disappears together with growing up an intense emission band central at ~505 nm. In 80% and 90% solutions, the fluorescence enhancement accompanies with the formation of nanobelts and emission bands shifts to ~518 nm. The strong fluorescence enhancement of nanobelts can be attributed to both intra- and intermolecular interactions. The intramolecular effect refers to the restriction of intramolecular motions in nanoaggregates.[2,3,45,46] The intermolecular effect arises from the interaction between aggregated molecules, which depends on the geometry of packing structures.[40] According to simple exciton model,[50] the emitting state in H-type aggregate is dipole-forbidden (or less allowed), and the fluorescence enhancement observed in this case is unique for H-type aggregates. To elucidate the unusual fluorescence enhancement mechanism, we have measured the fluorescence decays of CNDSB in various environments, and the results will be discussed.

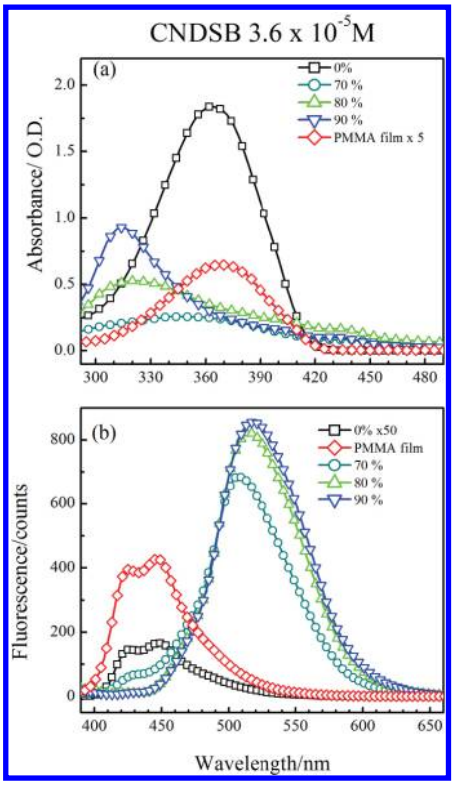

Figure 2. (a) UV–vis absorption and (b) emission spectra of CNDSB in various environments. The concentration of CNDSB was fixed at 3.6×10^{-5} M, and the weight percentage of CNDSB in PMMA film was controlled at 1:1000. For emission spectra, the excitation was fixed at 375 nm, and all intensity has been normalized according to the absorbance at 375 nm.

Picosecond Relaxation Dynamics of CNDSB Nanobelts. Figure 3 shows a series of time-resolved profiles of CNDSB in different environments. All transients are taken with

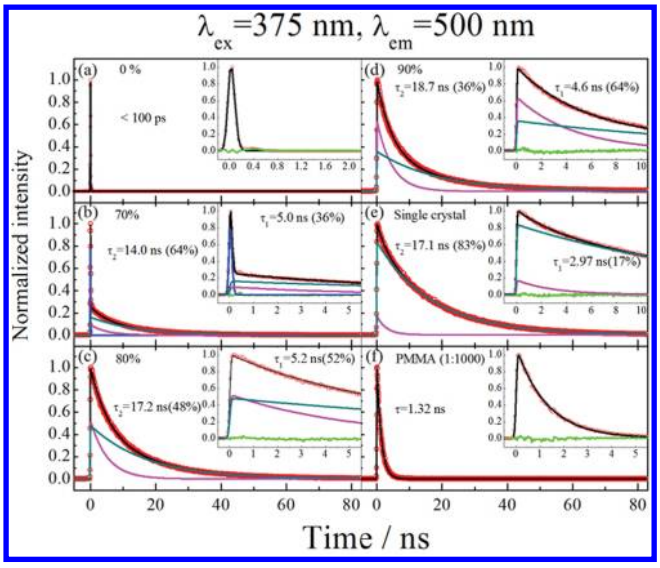

Figure 3. Picosecond transients of CNDSB in (a) 0%, (b) 70%, (c) 80%, (d) 90%, (e) single crystal, and (f) PMMA film. The relative amplitude of each component is indicated in the parentheses. The solid black curves are theoretical fits with residues shown as green traces; the deconvolution of each component is indicated by different colors.

dx.doi.org/10.1021/jp304117n | J. Phys. Chem. C 2012, 116, 15146–15154

TCSPC spectroscopy. The excitation and the emission wavelengths are fixed at 375 and 500 nm, respectively. In pure THF solution, the fluorescence decay is faster than the instrument response function of our system (~100 ps); hence, we only observed a sharp spike. In 70% solution, besides the spike observed in THF solution, an additional long component appeared in the transient. In 80% and 90% solutions, the sharp spike disappears and the long component becomes dominant. The increasing of fluorescence lifetime is correlated with the fluorescence enhancement and the formation of nanostructure in these solutions. Therefore, the nanosecond decay components are attributed to the emission from nanostructure. The dynamics of nanosecond component were fitted with a biexponential decay function. The fast component τ_1 is 4−5 ns while the slow component τ_2 varies from 14−19 ns. The biexponential decay suggests that at least two different structures coexist in these nanoaggregates. It should be noted that the amplitude of the fast component increases from 36% to 64% in 70%−90% solutions. The result is correlated with the formation of B-phase packing structure in high water volume percentage solutions. Therefore, the fast component τ_1 is ascribed to the emission from B-phase structure, while the second component τ_2 is attributed to the emission from G-phase structure. This assignment consists with the result reported by Park et al., in which they observed shorter fluorescence lifetime in B-phase structure.[40] In single crystal (Figure 3e), the amplitude of the fast component decreases substantially and the slow component τ_2 becomes dominate. This result reveals the different molecular packing structures between the nanobelts and single crystal.

Many reports for AIE phenomenon suggested that the restriction of intramolecular motion is the primary reason that should response for the observing fluorescence enhancement.[2,3,45,46] To prove this, we prepared a thin film of CNDSB in poly(methyl methacrylate) (PMMA) to mimic the rigid environment in solid state. The shape of the absorption and emission spectra of CNDSB in PMMA film (Figure 2a) is similar to what we observed in THF solution. In the meanwhile, the emission of CNDSB in PMMA film also closely resemble with the spectra of CNDSB/THF solution measured at cryogenic temperature (Figure S1). These results imply similar CNDSB conformations in these environments. In PMMA film, CNDSB emits strong fluorescence and the fluorescence decays single-exponentially with a time coefficient of 1.32 ns (Figure 3f). The inherent fluorescence lifetime of CNDSB in PMMA film is significantly longer than that in THF solution but much shorter than those in 70−90% solutions. It is interesting that CNDSB shows different fluorescence decay dynamics in PMMA film and nanobelts. If the fluorescence enhancement is simply due to the structural confinement, we should observe similar fluorescence decays for these two cases. The result suggests that the structural restriction effect can only partially explain the fluorescence enhancement of nanobelts. In H-type aggregates, the excited state is split into two different excitonic states due to the interaction between aggregate molecules.[50] Upon excitation, the molecule is excited to the transition allowed upper excitonic state while the fluorescence we observed is emitted from the transition forbidden lower excitonic state. Since the emitting state in nanobelt structure is intrinsically different from those of the isolated molecule, it is reasonable for us to expect different fluorescence lifetimes in these two cases. Recent study also suggests the radiative lifetime in H-type aggregate will be drastically slow down due to the dipole forbidden nature of the emitting state.[40,42,51] In the meanwhile, the change of energy gap and the different vibronic coupling efficiencies might also change the radiative lifetime significantly.[35] To further elucidate this issue, the molecular structures of CNDSB in a crystal and in THF solution were determined using X-ray diffraction spectroscopy and quantum-chemical calculation method, respectively, and the results will be discussed in next section.

Molecular Structures of CNDSB in Solid State. Figure 4a shows the crystal structure of CNDSB. The general formula

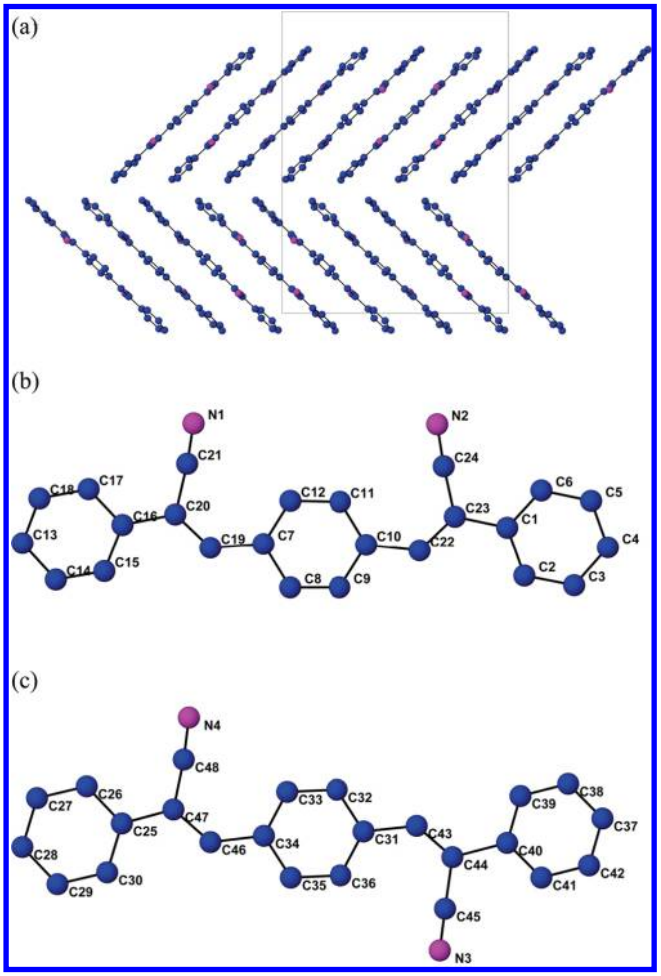

Figure 4. (a) Projection of the structure viewed along the [010] direction showing herringbone arrangement of CNDSB molecules. (b) The front view of *cis*-CNDSB molecules with the atomic numbering scheme. Blue circles: C. Red Circles: N. Hydrogen atoms are omitted for clarity. (c) The front view of *trans*-DSB molecules with the atomic numbering scheme. Blue circles: C. Red Circles: N. Hydrogen atoms are omitted for clarity.

for CNDSB is $(C_6H_5)_2(C_6H_4)(C_2HR_2)$. There are eight symmetry-related CNDSB molecules in a unit cell that can be reduced to two symmetry unique molecules, *cis*-(**1**) and *trans*-CNDSB (**2**), as depicted in Figures 4b and 4c, respectively. In general, the CNDSB molecule contains three benzene rings that are connected by two ethylene groups. Each ethylene group connects two benzene rings and two CN groups (R = CN). For conformation **1**, the CN groups are pointing in the same direction that is defined as the cis-form. Such a molecular structure is the same as the PPB (R = CH_3) molecule in the crystal form.[26] On the other hand, conformation **2** is the

dx.doi.org/10.1021/jp304117n | J. Phys. Chem. C 2012, 116, 15146−15154

structural isomer of **1** with the two CN groups pointing toward opposite direction, which is defined as the trans-form. In these two conformations, the central benzene ring connects two phenyl groups via the ethylene double bonds in 1,4-positions. The dihedral angle between the end phenyl and the central phenyl groups (based on least-squares planes of phenyl groups) of **1** and **2** are 10.7° and 9.5°, respectively, indicating near-planar molecular structure. The packing patterns of CNDSB molecules form the well-known herringbone packing extending along the *ac* plane. The herringbone angles of CNDSB were determined from the vectors of terminal carbons between C4−C13 (conformer **1**) and C28−C37 (conformer **2**). The calculated herringbone angle of CNDSB based on such a definition is 87.2°, giving a nearly perpendicular structural arrangement, which is quite different to that of PPB (166.9°).[26]

As a comparison, the ground-state structure of isolated CNDSB molecule is estimated by quantum chemical calculations. Figure 5 shows the structure optimized at the

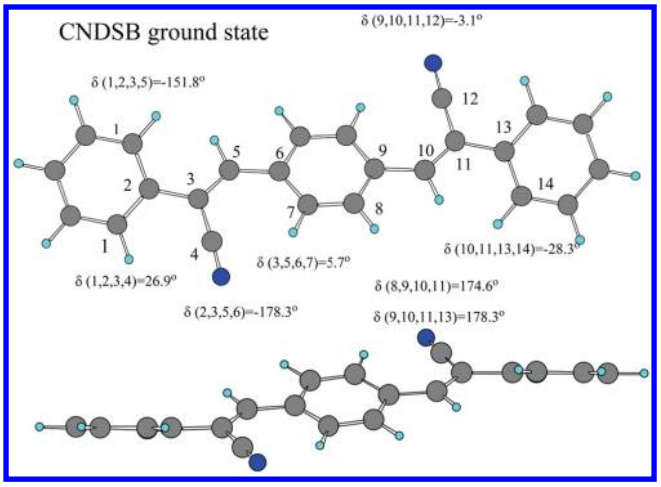

Figure 5. Ground-state structure of CNDSB optimized at the B3LYP/6-31G(d) level of theory; the side view is shown in the lower panel.

B3LYP/6-31G(d) level of theory using the Gaussian03 software package.[49] In contrast to the planar structure of distyrylbenzene,[26] the steric hindrance of the two CN moieties leads to the central benzene twisted by ∼30° relative to the plane formed by two other benzene rings. The twisted geometry of CNDSB results from the compromise effects between the π-conjugation and the steric hindrance. The vertical excitation energy of isolated CNDSB and the two isomers found in X-ray structure were estimated with TDDFT method at B3LYP/6-31G(d) level of theory. The results are tabulated in Table 2. The estimated excitation energy for isolated CNDSB (412 nm) is in good agreement with the 0−0 transition energy for CNDSB in THF solution (409 nm). In Table 2, we observed similar energy gaps in these three structures. Therefore, the planarization of CNDSB in crystal structure only has a minor effect on tuning the wavelength of steady-state absorption/emission spectra, and the drastic change we observed must arise from the intermolecular interaction between the nearby aggregated molecules as reported in PPB[26] and DBDCS.[40]

Femtosecond Relaxation Dynamics of CNDSB in THF Solution and Nanobelts. Femtosecond-resolved fluorescence up-conversion spectroscopy is applied to study the relaxation dynamics in the range between 0 and 150 ps. Figure 6a depicts the fluorescence transient of CNDSB in THF solution. The

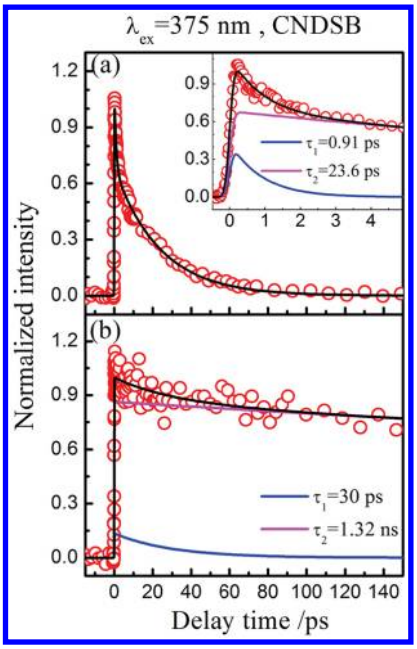

Figure 6. Femtosecond transients of CNDSB in (a) THF and (b) PMMA thin film. For CNDSB in THF solution, the transient was obtained at λ_{ex} = 375 nm and λ_{em} = 480 nm. For PMMA films, the transient was obtained at λ_{ex} = 375 nm and λ_{em} = 460 nm. The black solid line shows the biexponential curve of the transient. The deconvolution of transients was indicated by different colors. For consistency, the long decay component of CNDSB in PMMA film was fixed at 1.32 ns, which corresponded to the value obtained from TCSPC spectroscopy.

fluorescence decay is described by a biexponential decay function with time coefficients of 0.91 and 23.6 ps. Because of the structural similarity between CNDSB and *trans*-stilbene, the observed fluorescence dynamics can be interpreted accordingly. For isolated *trans*-stilbene, the relaxation dynamics in S_1 state are controlled by the C═C bond twisting motion toward the formation of cis-isomer with an energy barrier of only 14.2 kJ mol^{-1}.[52] The trans-to-cis isomerization in the S_1 state occurred on the time scale ranging from picoseconds to tens of picoseconds, depending on the available vibrational energy.[52] A similar isomerization process in PPB occurred in ∼1 ps;[26] thus, the observed 0.91 ps fast-decay component in CNDSB is attributed to the twisting motion along the C═C bonds. In THF solution, the solvent-induced vibrational relaxation also occurred during the isomerization process, giving the 23.6 ps slow-decay component observed in the transient (Figure 6a). For CNDSB in PMMA film (Figure 6b), the transient is also fitted with a biexponential function. The fast component is about 30 ps and the offset component is fixed at 1.32 ns according to the TCSPC result (Figure 3f). The absence of the sub-picosecond component is due to the restriction of large-amplitude intramolecular motions of CNDSB in solid matrix. The 30 ps component is attributed to the internal energy dissipation from the excited state of CNDSB to the PMMA matrix, which is similar to the energy transfer process reported for $[Ru(bpy)_3]^{2+}$ in PMMA films.[53]

Figure 7 shows the femtosecond-resolved fluorescence transients of the CNDSB nanobelts in 80% solution. These transients are taken at excitation wavelength λ_{ex} = 375 nm and probed at three different wavelengths (λ_{pr} = 460, 500, and 550 nm). Besides the offset corresponding to the nanosecond

dx.doi.org/10.1021/jp304117n | J. Phys. Chem. C 2012, 116, 15146−15154

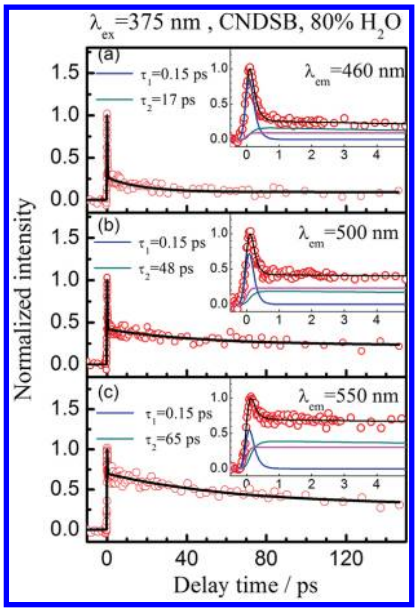

Figure 7. Femtosecond transients of CNDSB nanobelts in 80% water/THF solution; the excitation wavelength was fixed at 375 nm and probe at (a) 460, (b) 500, and (c) 550 nm. For each transient, at least three components were required to get the satisfactory fitting. The inset shows the deconvolution of each component. The longest component (magenta line) was fixed at the value obtained from TCSPC result.

components observed in Figure 3c, the residual parts of the transients are fitted with two exponential decay components. The first decay coefficient τ_1 is ~0.15 ps, and the second decay coefficient τ_2 varies from 17 to 65 ps. Because the decays of the first component are significantly faster than what we observed for CNDSB in THF solution, the emission contributed from the residual isolated CNDSB molecules in solution should be very minor. In order to ensure that the ultrafast decay component is not due to the scatting signal from the excitation pulses, we measured the fluorescence anisotropy dynamics at λ_{ex} = 375 nm and λ_{pr} = 500 nm; the results are shown in Figure 8. The existence of the ultrafast decay component in the transient of perpendicular polarization and the feature of time-independent emission anisotropy (~0.15) indicate that the observed 0.15 ps decay components must arise from the molecular response of CNDSB nanobelts. Such an ultrafast decay component is absent in the system of nanoparticles.[26] Our observation implies that there exists a rapid energy dissipation channel along the one-dimensional relaxation coordinate in belt-like structure, but this one-dimensional energy relaxation channel is inhibited in the case of organic nanoparticles. In H-type aggregate, the absorption and the emission occurred at different excitonic states.[50] An initial anisotropy of ~0.15 suggests that the internal conversion between the two excitonic states are too fast to be resolved by our system and the angle between the transition dipole of these two states can be estimated to be ~40.2°.[54] For the second decay coefficient τ_2, the dynamics are similar to what we observed in PPB nanoparticles. Accordingly, we attribute this 17−65 ps decay components to the energy transfer process caused by the intermolecular interactions of the $\pi-\pi$ stacking of the carbon backbones as in the case of PPB nanoparticles.[26]

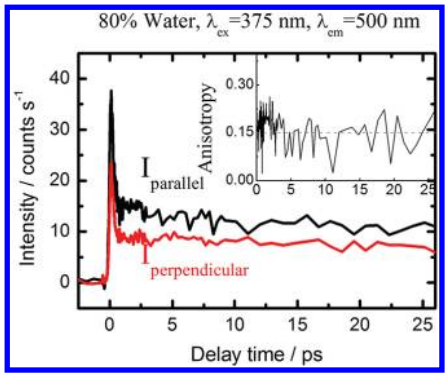

Figure 8. Anisotropy decay dynamics of CNDSB in 80% solution. The $I_{parallel}$ and $I_{perpendicular}$ indicate the polarization of the collecting fluorescence is parallel and perpendicular relative to the polarization of excitation beam, respectively. The anisotropy decay $r(t)$ was calculated using the equation $r(t) = [I_{parallel}(t) - I_{perpendicular}(t)]/[I_{parallel}(t) - 2I_{perpendicular}(t)]$.

CONCLUSION

In summary, we have synthesized an organic compound CNDSB which forms nanosize belt-like structure in high percentage water/THF solutions. This compound shows typical phenomena of AIE in solid phase. Our study suggested that both the structural restriction and intermolecular interaction are important for the observed fluorescence enhancement phenomenon. The dipole−dipole interactions between H-type aggregates greatly decrease the radiative rate of CNDSB nanobelts. Although the decreasing of radiative rate is deleterious for the overall fluorescence quantum yield, the structural restriction in solid state prohibits the possible nonradiative channel that competes with the radiative processes; therefore, we still observed a fluorescence enhancement in H-type aggregates. The fluorescence intensities of CNDSB are significantly enhanced in both PMMA film and nanobelts; the time-resolved spectral measurements reveal the different fluorescence decay dynamics in these two cases. The decay coefficients of isomerization and vibrational relaxation processes for CNDSB in THF solution have been estimated to be 0.91 and 23.6 ps, respectively. In nanobelt structure, we observed a unique ultrafast decay (time coefficient ~0.15 ps) along with an energy transfer processes in tens of picoseconds. The 0.15 ps decay component shown in the femtosecond transients of the CNDSB nanobelts is regarded as the ultrarapid energy dissipation process along the one-dimensional coordinate.

Scheme 2 shows the schematic presentation of the excited-state dynamics of isolated CNDSB and CNDSB nanobelts. For CNDSB in PMMA film, the fluorescence lifetime was estimated to be 1.32 ns. For the nanostructure formed in 70−80% solutions, the fluorescence shows a biexponential decay, and the result is ascribed to the different emissive structures in nanobelts. One is ranging from 14 to 19 ns, which represents the fluorescence arising from G-phase packing structure; another is ranging from 4 to 5 ns, which corresponds to emission from B phase pack structure. The substantially decreases of the fast component in single crystal also suggests the larger slip between the molecular sheet. In conclusion, our results clearly demonstrated how the excited-state dynamics of CNDSB changes in various environments. The versatile techniques used in this study thus have provided the essential information for the in-depth understanding of the spectral and the excited-state relaxation prosperities of the organic nano-

dx.doi.org/10.1021/jp304117n | J. Phys. Chem. C 2012, 116, 15146−15154

Scheme 2

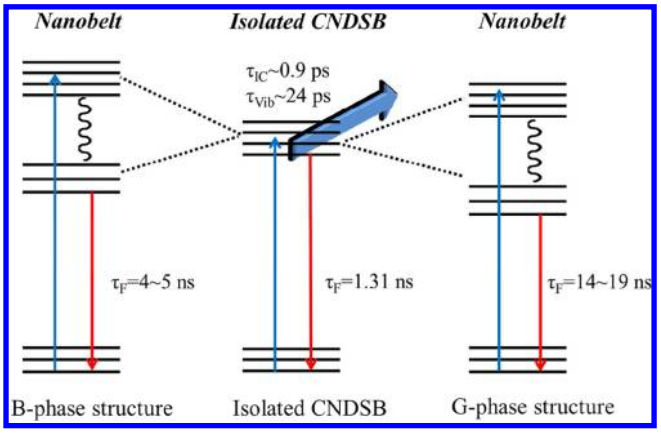

crystals of different morphologies featuring impressive AIE phenomena.

■ ASSOCIATED CONTENT

Supporting Information

CNDSB structure (.cif file); emission spectra of CNDSB/THF solution measured in cryogenic temperature (77 K) (Figure S1). This material is available free of charge via the Internet at http://pubs.acs.org.

■ AUTHOR INFORMATION

Corresponding Author

*E-mail: cwchang@cc.ncue.edu.tw (C.-W.C.); diau@mail.nctu.edu.tw (E.W.-G.D.).

Notes

The authors declare no competing financial interest.

■ ACKNOWLEDGMENTS

C. W. Chang thanks the National Science Council of Taiwan (Project Contract 100-2113-M-018-005-MY2) for financial support, and Eric W.-G. Diau thanks the National Science Council of Taiwan and Ministry of Education of Taiwan, under the ATU program, for providing support for this project.

■ REFERENCES

(1) Schlamp, M. C.; Peng, X.; Alivisatos, A. P. *J. Appl. Phys.* **1997**, *82*, 5837−5842.
(2) Tong, H.; Dong, Y. Q.; Hong, Y. N.; Haussler, M.; Lam, J. W. Y.; Sung, H. H. Y.; Yu, X. M.; Sun, J. X.; Williams, I. D.; Kwok, H. S.; Tang, B. Z. *J. Phys. Chem. C* **2007**, *111*, 2287−2294.
(3) Hong, Y. N.; Lam, J. W. Y.; Tang, B. Z. *Chem. Commun.* **2009**, 4332−4353.
(4) Shipway, A. N.; Katz, E.; Willner, I. *ChemPhysChem* **2000**, *1*, 18−52.
(5) Hong, Y. N.; Haussler, M.; Lam, J. W. Y.; Li, Z.; Sin, K. K.; Dong, Y. Q.; Tong, H.; Liu, J. Z.; Qin, A. J.; Renneberg, R.; Tang, B. Z. *Chem.—Eur. J.* **2008**, *14*, 6428−6437.
(6) Gonzalez-Rodriguez, D.; Janssen, P. G. A.; Martin-Rapun, R.; De Cat, I.; De Feyter, S.; Schenning, A.; Meijer, E. W. *J. Am. Chem. Soc.* **2010**, *132*, 4710−4719.
(7) Horn, D.; Rieger, J. *Angew. Chem., Int. Ed.* **2001**, *40*, 4330−4361.
(8) Silinsh, E. A. *Organic Molecular Crystals: Their Electronic States*; Springer-Verlag: Berlin, 1980.
(9) Alivistos, A. P. *Science* **1996**, *271*, 933−937.
(10) Forrest, S. *MRS Bull.* **2001**, *26*, 108−122.
(11) Peng, X.; Schlamp, M. C.; Kadavanich, A. V.; Alivisatos, A. P. *J. Am. Chem. Soc.* **1997**, *119*, 7019−7029.
(12) Chemla, D. S.; Zyss, J. *Nonlinear Optical Properties of Organic Molecules and Crystals*; Academic Press: Orlando, 1987; Vol. *1*.
(13) Gehr, R. J.; Boyd, R. W. *Chem. Mater.* **1996**, *8*, 1807−1819.
(14) Yoshikawa, H.; Masuhara, H. *J. Photochem. Photobiol., C* **2000**, *1*, 57−58.
(15) Raymond, J. E.; Ramakrishna, G.; Twieg, R. J.; Goodson, T. *J. Phys. Chem. C* **2008**, *112*, 7913−7921.
(16) Heng, L. P.; Wang, X. Y.; Tian, D. L.; Zhai, J.; Tang, B. Z.; Jiang, L. *Adv. Mater.* **2010**, *22*, 4716−4720.
(17) Figi, H.; Bale, D. H.; Szep, A.; Dalton, L. R.; Chen, A. T. *J. Opt. Soc. Am. B* **2011**, *28*, 2291−2300.
(18) Baba, K.; Kasai, H.; Okada, S.; Oikawa, H.; Nakanishi, H. *Opt. Mater.* **2002**, *21*, 591−594.
(19) Kasai, H.; Kamatani, H.; Okada, S.; Oikawa, H.; Matsuda, H.; Nakanishi, H. *Jpn. J. Appl. Phys.* **1996**, *35*, L221−L223.
(20) Kasai, H.; Nalwa, H. S.; Oikawa, H.; Okada, S.; Matsuda, H.; Minami, N.; Kakuta, A.; Ono, K.; Mukoh, A.; Nakanishi, H. *Jpn. J. Appl. Phys.* **1992**, *31*, 1132−1134.
(21) Katagi, H.; Kasai, H.; Okada, S.; Oikawa, H.; Komatsu, K.; Matsuda, H.; Liu, Z.; Nakanishi, H. *Jpn. J. Appl. Phys.* **1996**, *35*, L1364−L1366.
(22) Oikawa, H.; Mitsui, T.; Onodera, T.; Kasai, H.; Nakanishi, H.; Sekiguchi, T. *Jpn. J. Appl. Phys.* **2003**, *42*, L111−L113.
(23) Onodera, T.; Kasai, H.; Okada, S.; Oikawa, H.; Mizuno, K.-i.; Fujitsuka, M.; Ito, O.; Nakanishi, H. *Opt. Mater.* **2002**, *21*, 595−598.
(24) Takahashi, S.; Miura, H.; Kasai, H.; Okada, S.; Oikawa, H.; Nakanishi, H. *J. Am. Chem. Soc.* **2002**, *124*, 10944−10945.
(25) Fu, H.-B.; Yao, J. N. *J. Am. Chem. Soc.* **2001**, *123*, 1434−1439.
(26) Bhongale, C. J.; Chang, C.-W.; Lee, C.-S.; Diau, E. W.-G.; Hsu, C.-S. *J. Phys. Chem. B* **2005**, *109*, 13472−13482.
(27) Fu, H.; Loo, B. H.; Xiao, D.; Xie, R.; Ji, X.; Yao, J.; Zhang, B.; Zhang, L. *Angew. Chem., Int. Ed.* **2002**, *41*, 962−965.
(28) Kasai, H.; Kamatani, H.; Yoshikawa, Y.; Okada, S.; Oikawa, H.; Watanabe, A.; Itoh, O.; Nakanishi, H. *Chem. Lett.* **1997**, *26*, 1881−1882.
(29) Kuhn, H.; Försterling, H.-D. *Principles of Physical Chemistry, Understanding Molecules, Molecular Assemblies, Supramolecular Machines*; Wiley: New York, 2000.
(30) Belletete, M.; Bouchard, J.; Leclerc, M.; Durocher, G. *Macromolecules* **2005**, *38*, 880−887.
(31) Li, S.; He, L.; Xiong, F.; Li, Y.; Yang, G. *J. Phys. Chem. B* **2004**, *108*, 10887−10892.
(32) Ren, Y.; Lam, J. W. Y.; Dong, Y.; Tang, B. Z.; Wong, K. S. *J. Phys. Chem. B* **2005**, *109*, 1135−1140.
(33) Ren, Y.; Dong, Y.; Lam, J. W. Y.; Tang, B. Z.; Wong, K. S. *Chem. Phys. Lett.* **2005**, *402*, 468−473.
(34) Chen, J.; Law, C. C. W.; Lam, J. W. Y.; Dong, Y.; Lo, S. M. F.; Williams, I. D.; Zhu, D.; Tang, B. Z. *Chem. Mater.* **2003**, *15*, 1535−1546.
(35) Turro, N. J.; Ramamurthy, V.; Scaiano, J. C. *Principle of Molecular Photochemistry: An Introduction*; University Science Books: Sausalito, CA, 2009.
(36) Deans, R.; Kim, J.; Machacek, M. R.; Swager, T. M. *J. Am. Chem. Soc.* **2000**, *122*, 8565−8566.
(37) An, B.-K.; Kwon, S.-K.; Jung, S.-D.; Park, S. Y. *J. Am. Chem. Soc.* **2002**, *124*, 14410−14415.
(38) An, B.-K.; Lee, D.-S.; Lee, J.-S.; Park, S.-S.; Song, H.-S.; Park, S. Y. *J. Am. Chem. Soc.* **2004**, *126*, 10232−10233.
(39) An, B. K.; Gihm, S. H.; Chung, J. W.; Park, C. R.; Kwon, S. K.; Park, S. Y. *J. Am. Chem. Soc.* **2009**, *131*, 3950−3957.
(40) Yoon, S. J.; Chung, J. W.; Gierschner, J.; Kim, K. S.; Choi, M. G.; Kim, D.; Park, S. Y. *J. Am. Chem. Soc.* **2010**, *132*, 13675−13683.
(41) Kunzelman, J.; Kinami, M.; Crenshaw, B. R.; Protasievicz, J. D.; Weder, C. *Adv. Mater.* **2008**, *20*, 119−122.
(42) An, B.-K.; Gierschner, J.; Park, S. Y. *Acc. Chem. Res.* **2011**, *45*, 544−554.
(43) Dou, C.; Chen, D.; Iqbal, J.; Yuan, Y.; Zhang, H.; Wang, Y. *Langmuir* **2011**, *27*, 6323−6329.
(44) Li, X.; Xu, X.; Li, F.; Ma, Y. *Org. Electron.* **2012**, *13*, 762−766.

(45) Zeng, Q.; Li, Z.; Dong, Y. Q.; Di, C. A.; Qin, A. J.; Hong, Y. N.; Ji, L.; Zhu, Z. C.; Jim, C. K. W.; Yu, G.; Li, Q. Q.; Li, Z. A.; Liu, Y. Q.; Qin, J. G.; Tang, B. Z. *Chem. Commun.* **2007**, 70−72.
(46) Qian, Y.; Li, S. Y.; Zhang, G. Q.; Wang, Q.; Wang, S. Q.; Xu, H. J.; Li, C. Z.; Li, Y.; Yang, G. Q. *J. Phys. Chem. B* **2007**, *111*, 5861−5868.
(47) Bisht, P. B.; Fukuda, K.; Hirayama, S. *J. Phys. Chem. B* **1997**, *101*, 8054−8058.
(48) Pond, S. J. K.; Rumi, M.; Levin, M. D.; Parker, T. C.; Beljonne, D.; Day, M. W.; Brédas, J.-L.; Marder, S. R.; Perry, J. W. *J. Phys. Chem. A* **2002**, *106*, 11470−11480.
(49) Frisch, M. J.; Trucks, G. W.; Schlegel, H. B.; Scuseria, G. E.; Robb, M. A.; Cheeseman, J. R.; Montgomery, J. A., Jr.; Vreven, T.; Kudin, K. N.; Burant, J. C.; Millam, J. M.; Iyengar, S. S.; Tomasi, J.; Barone, V.; Mennucci, B.; Cossi, M.; Scalmani, G.; Rega, N.; Petersson, G. A.; Nakatsuji, H.; Hada, M.; Ehara, M.; Toyota, K.; Fukuda, R.; Hasegawa, J.; Ishida, M.; Nakajima, T.; Honda, Y.; Kitao, O.; Nakai, H.; Klene, M.; Li, X.; Knox, J. E.; Hratchian, H. P.; Cross, J. B.; Bakken, V.; Adamo, C.; Jaramillo, J.; Gomperts, R.; Stratmann, R. E.; Yazyev, O.; Austin, A. J.; Cammi, R.; Pomelli, C.; Ochterski, J. W.; Ayala, P. Y.; Morokuma, K.; Voth, G. A.; Salvador, P.; Dannenberg, J. J.; Zakrzewski, V. G.; Dapprich, S.; Daniels, A. D.; Strain, M. C.; Farkas, O.; Malick, D. K.; Rabuck, A. D.; Raghavachari, K.; Foresman, J. B.; Ortiz, J. V.; Cui, Q.; Baboul, A. G.; Clifford, S.; Cioslowski, J.; Stefanov, B. B.; Liu, G.; Liashenko, A.; Piskorz, P.; Komaromi, I.; Martin, R. L.; Fox, D. J.; Keith, T.; Al-Laham, M. A.; Peng, C. Y.; Nanayakkara, A.; Challacombe, M.; Gill, P. M. W.; Jhonson, B.; Chen, W.; Wong, M. W.; Gonzalez, C.; Pople, J. A. *Gaussian 03*, Revision B.5 ed.; Gaussian, Inc.: Wallingford, CT, 2004.
(50) Kasha, M.; Rawls, H. R.; El-Bayoumi, M. A. *Pure Appl. Chem.* **1965**, *11*, 371−392.
(51) Gierschner, J.; Ehni, M.; Egelhaaf, H.-J.; Medina, B. M.; Beljonne, D. *J. Chem. Phys.* **2005**, *123*, 144914.
(52) Baskin, J. S.; Bañares, L.; Pedersen, S.; Zewail, A. H. *J. Phys. Chem.* **1996**, *100*, 11920−11933.
(53) Chang, C.-W.; Chou, C. K.; Chang, I.-J.; Lee, Y.-P.; Diau, E. W.-G. *J. Phys. Chem. C* **2007**, *111*, 13288−13296.
(54) Valeur, B. *Molecular Fluorescence*; Wiley-VCH: New York, 2002.